A Comprehensive Theoretical Study on the Coupling Reaction Mechanism of Propylene Oxide with Carbon Dioxide Catalyzed by Copper(I) Cyanomethyl

Cai-Hong Guo,[†,‡] Hai-Shun Wu,*[,‡] Xian-Ming Zhang,[‡] Jiang-Yu Song,[‡] and Xiang Zhang[‡]

Chemical Engineering Department, Taiyuan University of Technology, Taiyuan 030024, China, and School of Chemistry and Materials Science, Shanxi Normal University, Linfen 041004, China

Received: October 26, 2008; Revised Manuscript Received: January 10, 2009

The mechanistic details of the coupling reaction of propylene oxide with carbon dioxide catalyzed by copper(I) cyanomethyl to yield cyclic carbonate were elucidated by density functional theory (DFT) calculations at the B3LYP/6-311G** level. Our results reveal that the overall reaction is stepwise and considered to include two processes. In process 1, CO_2 insertion into the Cu(I)−C bond of copper(I) cyanomethyl affords activated carbon dioxide carriers. In process 2, O-coordination of propylene oxide molecule to the electrophilic copper center of carriers occurs. Herein, three possible pathways were investigated, and the calculated reaction free energy profiles were compared. It was found that carrier **8** reacting with propylene oxide is more favored than the other two carriers (**6** and **7**) both kinetically and thermodynamically. Several factors, such as the composition of catalyst, the coordinate environment of copper, and the symmetry of frontier molecular orbitals, affected the reaction mechanisms, and the outcomes were identified. The overall reaction is exothermic. In addition, natural bond orbital (NBO) analysis has been performed to study the effects of charge transfer and understand the nature of different interactions between atoms and groups. The present theoretical study explains satisfactorily the early reported experimental observations well and provides a clear profile for the cycloaddition of carbon dioxide with propylene oxide promoted by $NCCH_2Cu$.

Introduction

Catalytic transformation of carbon dioxide (CO_2) into chemical products has attracted intense attention for the carbon source in industry and environmental problems.[1,2] One of the promising methodologies in chemical CO_2 fixation is the cycloaddition between carbon dioxide with epoxides to afford the five-membered cyclic carbonates, which are excellent aprotic polar solvents, fine chemical intermediates, and starting materials for the synthesis of polymers and engineering plastic.[3]

Various catalysts, especially metal complexes, have been continuously explored for the CO_2/epoxides coupling reactions over the past decades.[4] Some previous reports have suggested that parallel Lewis base activation of CO_2 and Lewis acid activation of epoxides should be important for the success of the reactions. For example, Cr(III), Cu(II), Co(II), and Zn(II) salen-type metal complexes can efficiently catalyze the reaction of epoxides with carbon dioxide to synthesize cyclic carbonates in high turnover frequency (TOF). Yet all of these catalyst systems are expensive, and catalyst reactivity is not high enough. It is also possible that the catalytic activity of Mg−Al mixed oxides in the coupling of carbon dioxide with epoxides originates from the cooperative action of neighboring basic and acidic sites on the surface of the catalyst. Later, a new, highly active, green $Ni(PPh_3)_2Cl_2/PPh_3/Zn$ catalyst system was reported for this reaction. Recently, Man et al. have synthesized heterobimetallic Ru−Mn complexes, which can catalyze the coupling reactions of epoxides with carbon dioxide efficiently for the first time, while they further performed the detailed calculations for the proposed mechanism at the B3LYP level of density functional theory. A key step in such reactions, as well as other chemical fixation reactions of CO_2, is activation of the unreactive CO_2 molecule with metal catalysts, such as insertion of CO_2 into the M−R (R = H, CH_3, or OR) bond of metal complexes.[5−13] Although many examples of the catalytic CO_2 conversion into organic chemicals were reported, the structure−activity relationship of the catalyst based on a reaction mechanism has not been fully understood.[14−19] In 1976, Saegusa et al. proposed that copper(I) cyanoacetate might act as a carrier of activated carbon dioxide in the coupling reactions of CO_2 with propylene oxide, and their studies showed that copper(I) cyanomethyl ($NCCH_2Cu$) is the effective catalyst for improving the yield of propylene carbonate.[15] However, the exact mechanism for the formation of propylene carbonate (Scheme 1) has not yet been elucidated partly due to the instability of $NCCH_2Cu$ under the experimental conditions. It should be noted here that in the past few years there have also been a few theoretical studies on transition-metal-mediated coupling reactions involving CO_2 and epoxides. For example, the mechanism of Zn(II)-catalyzed copolymerization of CO_2 with cyclohexene oxide was investigated with the hybrid molecular orbital method ONIOM.[31] Using alkylmethylimidazolium chlorine ([C*n*mim]Cl, n = 2, 4, and 6) as the catalyst, Sun et al.[32] studied the mechanism of the cycloaddition reaction of CO_2 with propylene oxide at the B3PW91/6-31G(d,p) level of density functional theory.

SCHEME 1

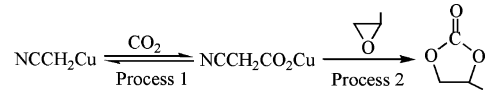

Thinking up mechanistic schemes that might explain such a robust process is an interesting but daunting challenge. While most "incredible" reactivity findings remain just that, the

* Corresponding author. Tel./fax: +86 357 2051375. E-mail: wuhs@dns.sxnu.edu.cn.
† Taiyuan University of Technology.
‡ Shanxi Normal University.

10.1021/jp809471s CCC: $40.75
Published on Web 05/26/2009

important and unprecedented intermediates are on the rare occasion proven bona fide. Moreover, what would be the reaction pathways? Which pathway is preferable? These arouse our great interest to investigate the reaction potential energy surfaces of propylene oxide with carbon dioxide catalyzed by copper(I) cyanomethyl. Thorough investigation on this reaction will be of important theoretical and practical value. Thus, in this work, we have performed detailed calculations using the B3LYP density functional theory (DFT) to study the full cycle of the catalytic reaction reported by Saegusa et al. (Scheme 1) in the gas phase. Our motif is to clarify the mechanism of the coupling reaction of carbon dioxide with propylene oxide, leading to propylene carbonate catalyzed by copper(I) cyanomethyl. At the same time, the detailed theoretical investigation should be helpful for us to understand the structural and energetic aspects of the possible reaction pathways.

The present computational study is, to the best of our knowledge, the first detailed comprehensive theoretical mechanistic investigation of the complete reaction cycle for the coupling reaction of carbon dioxide with propylene oxide catalyzed by copper(I) cyanomethyl. The structures of all intermediates and transition states involved in the processes have been located, and the relative energies of these species have been calculated. In addition, the natural bond orbital (NBO) analysis is also carried out to observe the bond order and charge changes in the process of the reactions.

Computational Details

All calculations were carried out using the Gaussian 03 program.[25] The geometries of the reactants, precursor complexes, transition states, intermediates, and products were fully optimized without constraints via DFT calculations using the B3LYP[20] functional. The B3LYP functional combines Becke's three-parameter nonlocal hybrid exchange potential with the nonlocal correlation functional of Lee, Yang, and Parr. Frequency calculations at the same level of theory were also carried out to confirm that the optimized structures were ground states without imaginary frequency (NImag = 0) or transition states with one imaginary frequency (NImag = 1). Especially, the lone imaginary frequency of each transition state displayed the desired displacement orientation, and intrinsic reaction coordinates (IRC)[21] were calculated for the transition states to confirm that such structures indeed connect two relevant minima. The 6-311G* Wachters−Hay basis set[22] was used for Cu atom, while the 6-311G** Pople basis set[23] was used for C, H, O, and N atoms. Zero-point energy corrections (ZPE), derived from the frequency calculations, were added to the total electronic energies of each species in the catalytic cycle. To match with the experimental conditions, all thermodynamic data reported in this Article were estimated at the temperature of 403.15 K and pressure of ca. 40 atm as presented in ref 15. This B3LYP method has been confirmed to be appropriate for copper(I)-catalyzed complex, as indicated by the excellent agreement in vibration frequencies and geometric parameters.[26,27,33] To obtain more reliable energies, additional single-point energy calculations were performed on some key species at the MP2/6-311+G** level. The zero-point and thermal energy corrections were made to the electronic and Gibbs free energies by using a scale factor of 0.963.[35] For interpretation purposes, Wiberg bond indexes and natural charges were also analyzed with the natural bond orbital (NBO) program.[24] The calculated total electronic energies, ZPEs, and thermal corrections to enthalpies and Gibbs free energies are provided in the Supporting Information.

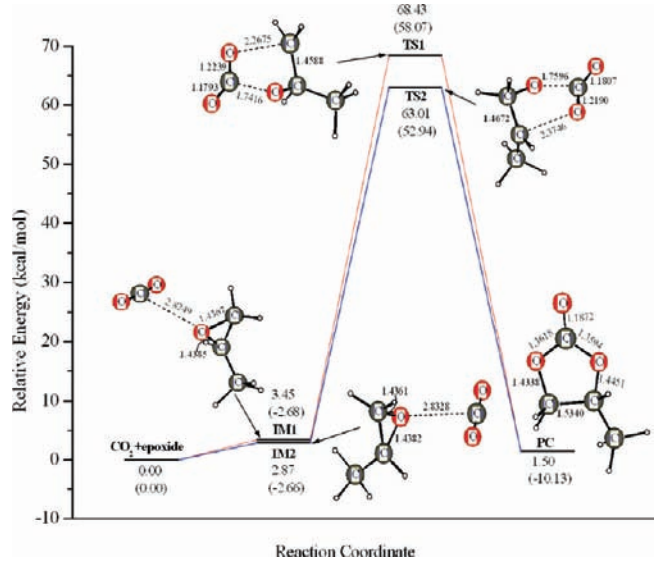

Figure 1. The calculated relative free energies (kcal/mol) and the relative electronic energies (in parentheses) of the species involved in the concerted cycloaddition reaction of CO_2 with propylene oxide in the absence of copper(I) cyanomethyl at 403.15 K and 40 atm.

Results and Discussion

As we know, the relative free energies (kcal/mol) and relative electronic energies (kcal/mol, in parentheses) are similar in the cases where the number of reactant and product molecules is equal, that is, one-to-one or two-to-two transformations, but different significantly for one-to-two or two-to-one transformations because of entropic contributions. To take into account the effect of entropy, we use the free energies (ΔG) of activation and reaction, and the corresponding enthalpies (ΔH) to analyze the reaction mechanism in our discussion.

The Uncatalyzed, Concerted Cycloaddition. The geometries of reactants (CO_2 and propylene oxide), two dimolecular complexes, two different transition states, and product (propylene carbonate) were optimized at the B3LYP/6-311G** level. The corresponding geometrical structures and Cartesian coordinates are presented in the Supporting Information.

Initially, two dimolecular complexes between CO_2 and propylene oxide (see **IM1** and **IM2** in Figure S1) were formed via the weak van der Waals interaction, as indicated by the $C_{carbondioxide}-O_{epoxide}$ distances (2.8249 and 2.8328 Å) and small binding energies (2.68 and 2.66 kcal/mol) between two reactants. As shown in Figure 1, two different five-membered ring transition states, **TS1** and **TS2**, have been located. In **TS1**, the $C_{epoxide}-O_{epoxide}$ bond is practically broken (2.0156 Å), whereas two new bonds start to form, the $C_{carbondioxide}-O_{epoxide}$ bond (1.7416 Å) and $C_{epoxide}-O_{carbondioxide}$ bond (2.2675 Å), while the corresponding ones in **TS2** are 2.0913, 1.7596, and 2.3746 Å. The imaginary frequencies associated with **TS1** and **TS2** are 682.13 and 577.71i cm^{-1}; these values are slightly lower than that of the corresponding transition states predicted by Sun et al.[32] The analysis of the vibrational modes clearly indicates that both pathways of the cycloaddition reaction to afford the five-membered cyclic propylene carbonate proceed via a concerted mechanism.

The electronic energy and free energy profiles along the reaction coordinate with the optimized structures of the dimolecular complexes and transition states involved in the reaction are displayed in Figure 1. One can see that the activation barrier from **IM1** to **TS1** or from **IM2** to **TS2** is calculated to be as high as 64.98 or 60.14 kcal/mol in the gas phase (403.15 K and 40 atm), which implies that this uncatalyzed coupling

SCHEME 2: Proposed Reaction Pathways for the Carboxylation of Cyanomethylcopper in Process 1

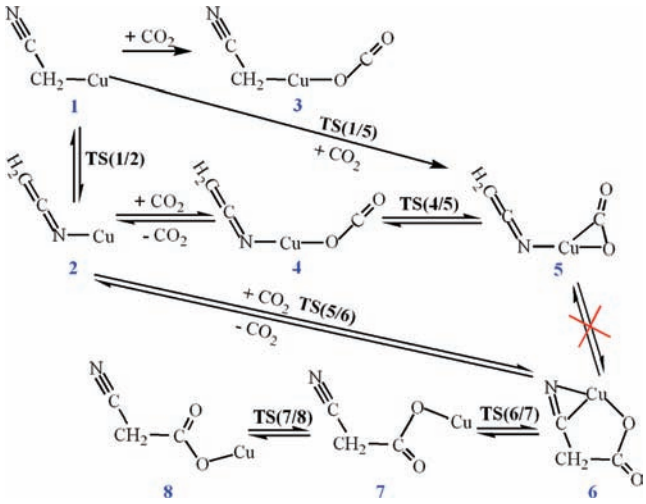

reaction has an insurmountable barrier. The overall concerted cycloaddition reaction is exothermic by 11.31 kcal/mol, but endergonic by 1.50 kcal/mol. On the basis of the above data, it is concluded that the uncatalyzed, concerted reaction is not accessible thermodynamically and kinetically.

The Cu(I)-Catalyzed Reaction Mechanism. In our work, all of the relevant stationary points have been located at the B3LYP/6-311G** (6-311G* for Cu atom) level. Our results shed light on that the title reaction should be considered to include two reaction processes.

Process 1: Formation of Copper(I) Cyanoacetate. As mentioned in the Introduction, the activation of CO_2 by copper(I) cyanomethyl is a very important process (Scheme 2). The catalytic cycle begins with the activating of linear carbon dioxide molecule by the active catalyst $NCCH_2Cu$. Because copper(I) cyanomethyl can exist in two different isomeric forms depending on the coordination of the CH_2CN ligand (see **1** and **2** in Scheme 2), there should be various configurations of the activated carbon dioxide carrier. On the potential energy surfaces (PES) of the reaction of CO_2 with copper(I) cyanomethyl in the gas phase, we have located five different transition states and six intermediates. The corresponding optimized structures and selected parameters are depicted in Figure 2.

As shown in Scheme 2, one pathway (**1** + CO_2 → **2** + CO_2 → **4** → **5** → **6** → **7** → **8**) in process 1 was first investigated and discussed. The first step is that $NCCH_2Cu$ undergoes a rearrangement from **1** to **2**, a less stable isomer of **1**; the second step is the nucleophilic attack of $O_{carbon\ dioxide}$ atom to the Cu atom of species **2** to afford complex **4**; the third step is the formation of a side-on complex **5** via **TS(4/5)**; the next step is an isomerization step from complex **5** to five-membered cyclic intermediate **6** surpassing **TS(5/6)**; the following step corresponds to the torsion of copper of intermediate **6** leading to intermediate **7**; the last step is a tautomerization step from **7** to **8** overcoming **TS(7/8)**. In reactant **1**, from Figure 2, the lengths of the Cu−C_1, C_1−C_2, and C_2−N bonds are 1.8824, 1.4401, and 1.1570 Å. The Wiberg bond index of Cu−C is 0.77 with NBO analysis. In the first step, the transition state **TS(1/2)** has been located. The Cu−C_1, Cu−C_2, and Cu−N distances are 2.5336, 1.9856, and 2.0174 Å, respectively. The imaginary frequency is 454.07i cm^{-1}, which exactly corresponds to the rotation mode of η^3-CH_2CN in the plane. The energy barrier from **1** to **TS(1/2)** is 40.55 kcal/mol. For structure **2**, the lengths of Cu−N, C_1−C_2, and C_2−N bonds are 1.8133, 1.3283, and 1.2060 Å, respectively; Cu−N, C_1−C_2, and C_2−N bond indices are 0.5828, 1.3444, and 1.6264, which implies that the Cu−N bond and C_1−C_2 double bond have been completely formed and the C_2−N triple bond is weakened. From the energy profile shown in Figure 3, we can see that the rearrangement step (**1** → **2**) is endergonic by 17.26 kcal/mol and endothermic by 17.54 kcal/mol (see Table S1). Therefore, starting from **1** + CO_2, the process can undergo an isomerization step followed by the reaction of **2** with CO_2 or proceed directly through the reaction between **1** and carbon dioxide.

As depicted in Scheme 2, two end-on-coordination carbon dioxide complexes (**3** and **4** in Figure 2) were predicted to be the direct products in the reaction of CO_2 with **1** (or **2**). One can see from Table S1 that complex **3** is more stable than the separated reactants (**1** + CO_2) by 17.91 kcal/mol, while the formation of complex **3** is exoenergic by 10.84 kcal/mol. It is concluded that this is a spontaneous step. However, from the energy profile in Figure 3, we can find that the production of complex **4** is endergonic by 4.79 kcal/mol, although it is more stable by 2.85 kcal/mol than the separated reactants (**1** + CO_2). Wiberg bond indices of Cu−$O_{carbondioxide}$ (0.1341, 0.1323 for **3**, **4**) indicate the weak back-donative interaction between Cu 3d orbital and CO_2 π^* orbital. Herein, both were stabilized by the strong electrostatic interaction between positively charged Cu atom and the negatively charged O atom of carbon dioxide. Note that complexes **3** and **4** are not the effective carriers of activated carbon dioxide molecule from the almost unchanged geometry of CO_2. Interestingly, complex **4** is highly reactive to proceed partly due to the exposition of the CH_2 moiety; on the other hand, the larger natural charge (+0.701 *e*) on the Cu atom in **4** can induce the side-on coordinate of carbon dioxide. In contrast with species **4**, the natural charge (+0.618 *e*) on the Cu atom in complex **3** is relatively smaller, and the coordination of $C_{methylene}$ atom is nearly saturated, which result in the unreactivity of species **3**. Thus, we further investigated the transformation of complex **4** under high temperature and pressure. Several activated carbon dioxide carriers were located afterward.

As displayed in Scheme 2, one side-on-coordination carbon dioxide complex (**5** in Figure 2) was optimized. At this stage, it should be mentioned that similar attempts to optimize a η^2-C,O side-on structure directly starting from **1** + CO_2 were unsuccessful. Only the η^1-O end-on structure **3** was converged, which seems to be consistent with the characterized XCuOCO (X = Cl and Br) by Zhou et al.[34] We then located an authentic transition state **TS(4/5)**, which connects with complexes **4** and **5**. The Cu−N, Cu−C_3, Cu−O_1, and O_1−C_3 distances in **TS(4/5)** are 1.8100, 2.5240, 1.9313, and 1.1836 Å, respectively. The Cu−O_1−C_3 bond angle is 105.73°. It is indicated that the transition state **TS(4/5)** has the trend to produce a side-on-coordinated carbon dioxide complex because of the ability of Cu(I) to provide π back-donation and the ability of $C_{carbondioxide}$ to accept electrons into the antibonding orbitals. The imaginary frequency is 73.05i cm^{-1}. The analysis of the vibrational modes indicates that this imaginary frequency is associated with the Cu−C_3 stretching motion. The calculated energy barrier from **4** to **TS(4/5)** is 0.93 kcal/mol, which is so low that this transition state is very easy to surpass after heating. Wiberg bond indices of Cu−C_3, Cu−O_1, O_1−C_3, and O_2−C_3 bonds change from 0.0474, 0.1323, 1.7127, and 1.9929 in **4** to 0.2991, 0.1819, 1.5911, and 1.9142 in **5**. For complex **5**, the O_1−C_3 and O_2−C_3 bond lengths are 1.2148 and 1.1648 Å, which are 0.0461 and 0.0138 Å longer than those in **4**. The O_1−C_3−O_2 bond angle is 158.98°. It is implied that the carbon dioxide molecule was

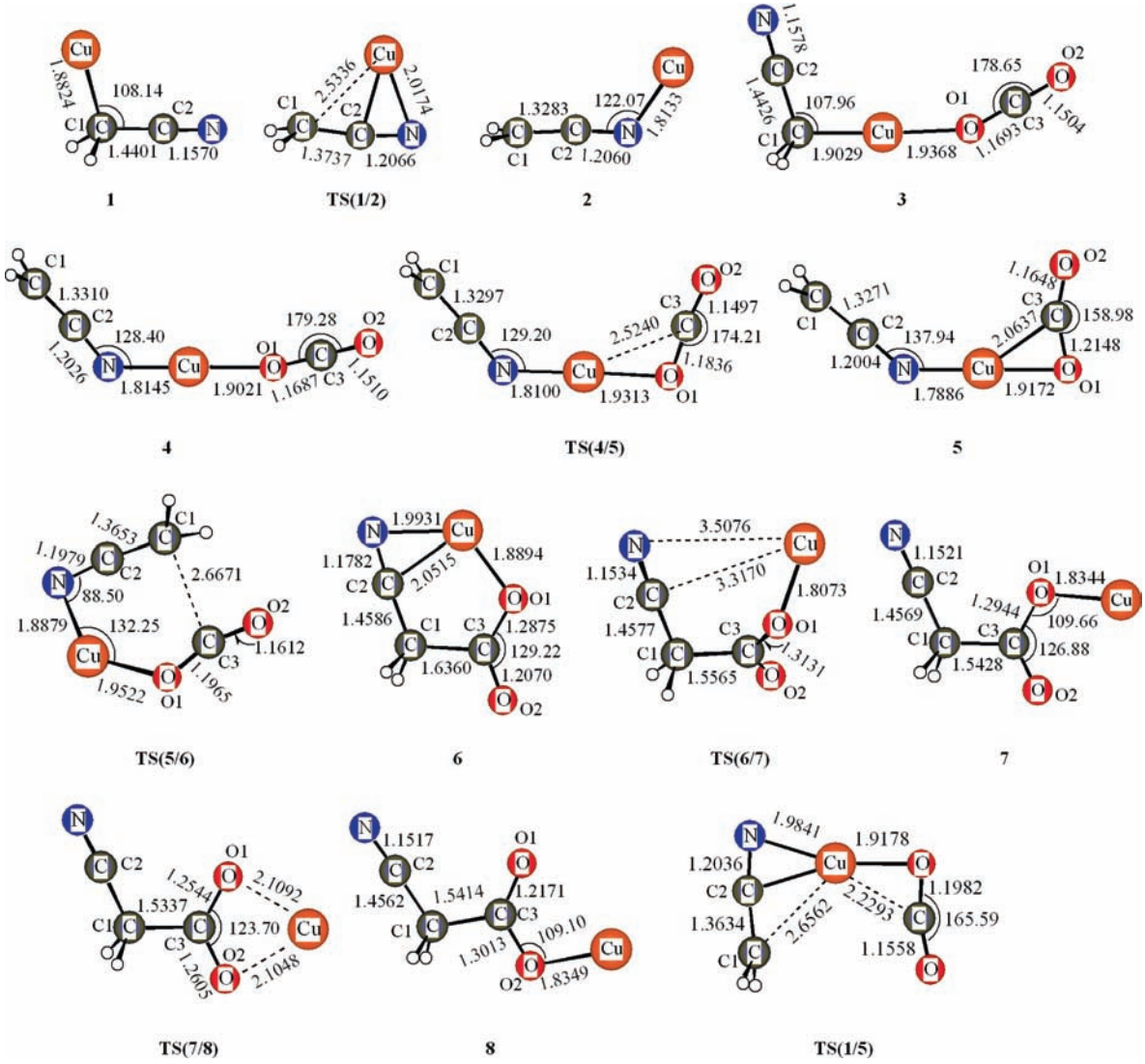

Figure 2. Optimized geometries (bond length, Å; bond angle, deg) in process 1 at the B3LYP/6-311G** level.

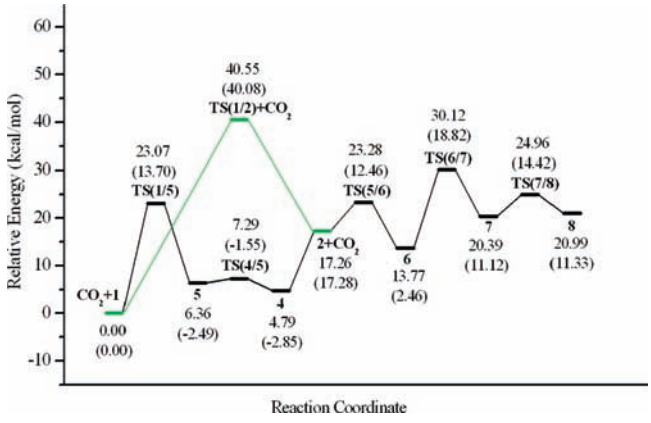

Figure 3. Free energies profiles (kcal/mol, in gas phase) for the reaction of $CuCH_2CN$ with CO_2 in process 1. The calculated relative electronic energies (values in parentheses) are also given.

activated in complex **5**. From **5**, we suppose that the C_3 atom can interact with electronegative C_1 atom when they move toward one another under high temperature. To verify this supposition, we have located only one transition state **TS(5/6)**. IRC calculations from **TS(5/6)** reveal that the located transition state is indeed associated with intermediate **6** in one direction; however, that in the other direction does not correspond to the complex **5** but to the dissociation of CO_2 from the metal center, that is, to **2** + CO_2 asymptote. Thus, the path **1** + CO_2 → **2** + CO_2 → **4** → **5** → **6** → **7** → **8** does not proceed, while the alternative path **1** + CO_2 → **2** + CO_2 → **6** → **7** → **8** will go ahead. The energy barrier from **2** + CO_2 to **TS(5/6)** is 6.02 kcal/mol. After the reaction surmounted the transition state **TS(5/6)**, the geometry **6** is produced. For complex **6**, as shown in Figure 2, one can see that the Cu atom interacts with O_1, C_2, and N atoms. Wiberg bond indices of Cu−N, Cu−C_2, Cu−O_1, C_3−O_1, and C_3−C_1 bonds are 0.2217, 0.2075, 0.2492, 1.2857, and 0.8315, respectively. The O_1−C_3 and O_2−C_3 bond lengths in **6** are 1.2875 and 1.2070 Å, which are 0.0727 and 0.0422 Å longer than those in **5**. The O_1−C_3−O_2 bond angle is 129.22°. These results show that the carbon dioxide was further activated in complex **6**. In the following step, we guess that the Cu atom could rotate about 180° around C_3−O_1 to be exposed. To verify our supposition, the authentic transition state **TS(6/7)** was located. The Cu−N, Cu−C_2, and C_3−O_1 distances in **TS(6/7)** are 3.5076, 3.3170, and 1.3131 Å, respectively. The Cu−O_1 bond length is 1.8073 Å, which is slightly shorter than that in **6**. It should be noted that the C_2, O_1, C_3, O_2, and H_4 atoms are almost on the same plane. The Cu−O_1−C_3−C_1 dihedral angle is −101.3°; the imaginary frequency is 72.87i cm^{-1}, which corresponds to the torsion of Cu atom around C_3−O_1 bond. The

energy barrier from **6** to **TS(6/7)** is 16.35 kcal/mol. After the reaction overcame the transition state **TS(6/7)**, complex **7** is formed. For geometry **7**, Wiberg bond indices of $Cu-O_1$, C_3-O_1, C_3-O_2, and C_1-C_3 bonds are 0.4165, 1.2486, 1.6419, and 0.9159. Note that the O_1-C_3 and O_2-C_3 bond lengths in **7** are 1.2944 and 1.2207 Å, which are 0.0069 and 0.0137 Å longer than those in **6**; the $O_1-C_3-O_2$ bond angle is 126.88°, which is shorter by 2.34° than that in complex **6**. It is indicated that the carbon dioxide was activated very well in geometry **7**. Complex **8** would be generated if the reaction surpassed the transition state **TS(7/8)**. In **TS(7/8)**, the $Cu-O_1$ bond distance was lengthened, while the $Cu-O_2$ bond distance was shortened. The imaginary frequency is 188.77i cm^{-1}, which is associated with the pseudorotation of copper atom. In geometry **8**, the $Cu-O_2$, C_3-O_1, and C_3-O_2 bond distances are 1.8349, 1.2171, and 1.3013 Å. The $O_1-C_3-O_2$ and $Cu-O_2-C_3$ bond angles are 126.67° and 109.10°, which are similar to those in complex **7**. The Wiberg bond index of $Cu-O_2$ bond in **8** is 0.4195, which is slightly larger than that of the $Cu-O_1$ bond in **7**. The calculated electronic energy shows that species **8** is 0.22 kcal/mol slightly higher than **7**. The energy barrier from **7** to **8** is 4.57 kcal/mol. It is implied that the isomerization process from **7** to **8** easily takes place.

On the basis of the energetics of path **1** + CO_2 → **2** + CO_2 → **6** → **7** → **8** in process 1, the first step (**1** → **2**) has too much difficulty occurring because of the high barrier of 40.55 kcal/mol. Thus, another reaction course, that is, the direct insertion of CO_2 into the Cu−C bond, has been investigated. All of our attempts to optimize a four-membered ring transition state for CO_2 insertion into the Cu−C bond failed. Only the transition state **TS(1/5)** (in Figure 2) was located. The imaginary frequency is 236.95i cm^{-1}. The corresponding imagarnary vibrational mode indicates that the transition state **TS(1/5)** has the trend to produce the side-on complex **5**. IRC calculation confirms that the side-on attack of CO_2 is accompanied by a simultaneous cleavage of $Cu-C_1$. If the reaction surmounted the transition state **TS(1/5)**, complex **5** would be generated. The energy barrier from the reactants (**1** + CO_2) to **TS(1/5)** is 23.07 kcal/mol, which is lower than that from **1** to **TS(1/2)**. This implies a rearrangement from **1** to **2** has no chance of occurring in the reaction. Therefore, the first step in process 1 is the formation of complex **5** by the directly side-on attack of carbon dioxide to species **1**. Subsequently, the side-on-coordination carbon dioxide complex **5** is transformed into the more stable end-on-coordination carbon dioxide complex **4**; this step is exoergic by 1.57 kcal/mol with an energy barrier of 0.83 kcal/mol. Next, species **2** is produced by the release of CO_2 from **4**. The following steps are just the same with the latter steps starting from **2** in the alternative path. Hereby, process 1 actually proceeds via six steps (**1** + CO_2 → **5** → **4** → **2** + CO_2 → **6** → **7** → **8**).

The schematic electronic energy and free energy profiles for process 1 are presented in Figure 3. Note that the Gibbs free energy difference between **8** and **7** is predicted to be 0.60 kcal/mol by using B3LYP functional. A more reliable calculation is necessary for the definite identification of the relative stabilities of them. Thus, we have performed single-point energy calculations on species **7** and **8** at the MP2/6-311+G** level. The MP2 Gibbs free energy difference between **8** and **7** is 0.63 kcal/mol. Therefore, both methods give the same trend of the stabilities of **8** and **7**. From Figure 3, one can see that the energy increases from the reactants ($NCCH_2Cu$ + CO_2) to the activated carbon dioxide carriers (**6**, **7**, and **8**), which implies that the formation of complex **6** (**7** or **8**) is an unspontaneous and endothermic process. Results indicate that the first step **1** + CO_2 → **5** is the rate-limited step in this process.

In view of the reaction energy barriers for the formation of complexes **6**, **7**, and **8** and relative energies between **6**, **7**, and **8**, it is noteworthy that **6**, **7**, and **8** may be the possible activated carbon dioxide carriers under high temperature and pressure conditions. Which of them is the best activated carbon dioxide carrier? We must further investigate their reactivity in process 2.

Process 2: Formation of Propylene Carbonate (4-Methyl-[1,3]dioxolan-2-one). In this portion of the study, we have investigated three possible pathways of the reaction between propylene oxide with copper(I) cyanoacetate for producing 4-methyl-[1,3]dioxolan-2-one. To state the reaction mechanism for process 2, three pathways were denoted as path 1 (the activated carbon dioxide carrier **6** being reacted to epoxide; see Scheme S1), path 2 (the more active carbon dioxide carrier **7** being reacted to epoxide; see Scheme S2), and path 3 (the most active carbon dioxide carrier **8** being reacted to epoxide; see Scheme S3) in this Article. It is clearly shown that each reaction path involves four major elementary steps: (i) epoxide coordination, (ii) ring-opening of epoxide, (iii) eight-membered ring intermediate oxidation transformation, and (iv) ring-closure of the cyclic carbonate coordinated to the copper center through the oxygen atom and the catalyst regeneration. In the following sections, the structures and energies of the intermediates and transition states involved in the three postulated mechanism are first discussed, and then the free energy surfaces are constructed for each reaction path. For the sake of immediately comparing the relative free energies of the stationary points standing on various pathways of three mechanisms, all of the relative free energies of the stationary points are referenced to the free energies of CO_2 + **1** ($NCCH_2Cu$) + epoxide. In light of these results, a comparison of the three mechanisms is addressed.

Path 1. We first discuss the case where a propylene oxide molecule coordinates to the electrophilic copper center of the most stable activated carbon dioxide carrier **6** through the $O_{epoxide}$ atom to afford precursor complexes (**6a**, **6b**, **6c**, and **6d**). The corresponding structures and selected parameters are displayed in Figure 4. There are two orientations for the propylene oxide coordination: (i) the methyl group is relatively far away from carrier **6**; and (ii) the methyl group is close to carrier **6**. Because of the orientation of the methyl group in propylene oxide, there are two isomers for each type of complex. For type (i) complexes, **6a** and **6b** are a pair of degenerated enantiomers. For type (ii) complexes, **6c** and **6d**, another pair of enantiomers, are also isoenergetic. As depicted in Figure 4 and Table S2, it is evident that the formation of both types of complexes is accessible thermodynamically and kinetically. Wherein complexes **6a** and **6b** are less stable than complexes **6c** and **6d** by 0.70 kcal/mol, the former are more slightly favored than the latter by 0.05 kcal/mol kinetically. Apart from the proposed qualitative orbital interaction of donation and back-donation by Versluis et al.,[28] the energy difference can be mainly of electronic effect other than steric origin of the methyl group from the frontier molecular orbitals for both type (i) and type (ii) complexes. The distance of the $Cu-O_{epoxide}$ bond in type (ii) complexes is almost equal to that in type (i) complexes, which may be partly due to the electronic effect of the electron-donating methyl group. On account of the small energy difference between type (i) and type (ii) complexes, we have analyzed their interconversion through the rotation of propylene oxide. As expected, we found two transition states, **TS(6b/6c)** and **TS(6d/6a)**, with only one imaginary frequency for **6b** to **6c** and **6d** to **6a**. The related barriers are 5.87 and 5.81 kcal/

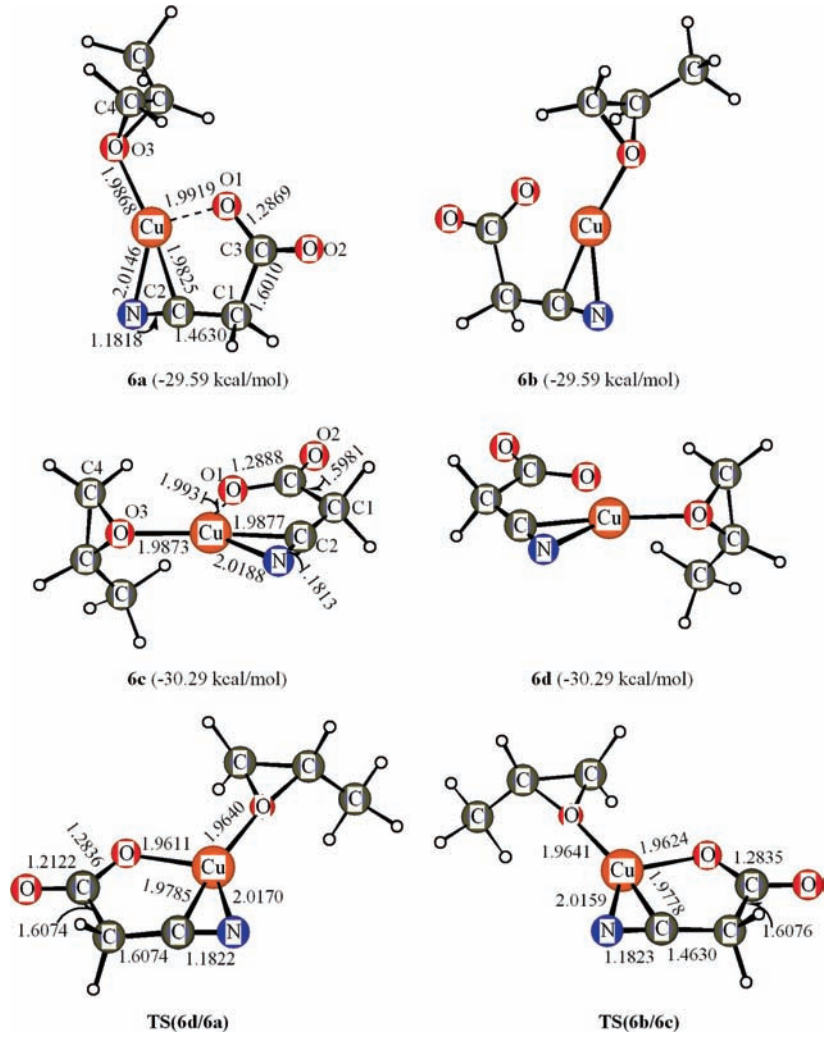

Figure 4. Optimized geometries of epoxide coordination complexes via oxygen atom interacting with carrier **6** and selected parameters. The bond lengths are given in angstroms.

mol, respectively. It is interesting to point out that only structures **6a** and **6c** are suitable for the subsequent ring-opening of the epoxide, which will be proved in the following steps. Therefore, complexes **6b** and **6d** should be transformed into **6c** and **6a** by all means. As a result, there are only two isomers (**6a** and **6c**) in the reaction system (**6** + epoxide). More interestingly, although complex **6a** is slightly less stable than **6c**, the former obviously facilitates the subsequent reaction of the ring-opening of epoxide. In complex **6a**, the $O_{epoxide}-C_4$ bond is more activated than that in **6c**, indicated by the longer C_4-O_3 bond length (1.4632 vs 1.4622 Å) with respect to that of 1.4326 Å in the free propylene oxide. To testify the reactivity of **6a** and **6c**, we have analyzed two sub-branched pathways in detail.

Subsequently, the ring-opening of the epoxide in complexes **6a** and **6c** may occur via two channels, that is, path 1-A and path 1-B. The optimized geometries and selected parameters are illustrated in Figures 5 and 6. Two transition states **TS(6a/9)** (in Figure 5) and **TS(6c/12)** (in Figure 6) have been located. The imaginary vibration mode indicates CH_2 carbon attacks near the oxygen atom of carbon dioxide, which leads to the cleavage of $C_4-O_{epoxide}$ and the formation of an eight-membered ring intermediate. IRC calculations confirm that **TS(6a/9)** connects **6a** and **9**, while **TS(6c/12)** connects **6c** and **12**. From **6a** to **TS(6a/9)**, the activation energy barrier is 38.13 kcal/mol; from **6c** to **TS(6c/12)**, the calculated energy barrier is 38.07 kcal/mol. After the reaction surmounted the transition state **TS(6a/9)** or **TS(6c/12)**, the intermediate **9** or **12** is produced. The intermediate **9** is slightly more stable than the intermediate **12** by 0.16 kcal/mol. This process is predicted to be exothermic by 2.86 (**6a** → **9**) or 2.51 (**6c** → **12**) kcal/mol. In view of the reaction energy barrier and the relative reaction energy for this step, it is difficult to choose which sub-branched path is favorable. Taking into account the tautomerization of species **9** (or **12**), we guess Cu atom may be transferred from cyano N to C_3 atom in the next step. Under our hypothesis, the transition states **TS(9/10)** and **TS(12/13)** were located. IRC results indicate that the migration of Cu atom to C_3 is accompanied by a simultaneous cleavage of C_3-C_1. After the reaction overcame **TS(9/10)** or **TS(12/13)**, the corresponding six-membered ring intermediate **10** or **13** is formed. This step is endothermic by 20.96 (**9** → **10**) or 21.33 (**12** → **13**) kcal/mol, with the activation energy of 36.17 or 36.05 kcal/mol, respectively. The intermediate **10** is also slightly more stable than the intermediate **13** by 0.49 kcal/mol. Here, from the optimized Cartesian coordinates of intermediates **10** and **13**, it is noted that the position of the methyl group in **13** indeed differs from that in **10**. We tried to locate the transition state connecting with **13** and the product complex heaps of times, but we failed; that is to say, intermediate **13** is not in favor of the reaction to proceed due to the greater steric hindrance of methyl group. Therefore, path 1-A is the only route for isolated reactants (**6** + epoxide) to proceed.

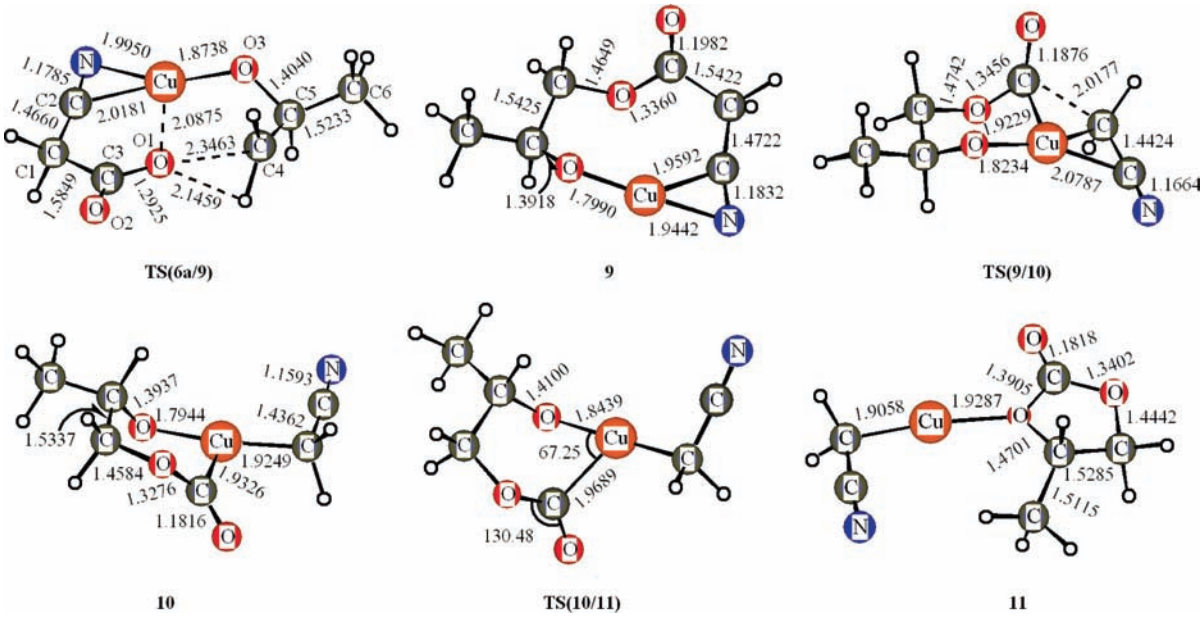

Figure 5. Key structures involved in the mechanism of the reaction of propylene oxide with carbon dioxide carrier **6** in the gas phase and selected parameters. The bond lengths are given in angstroms.

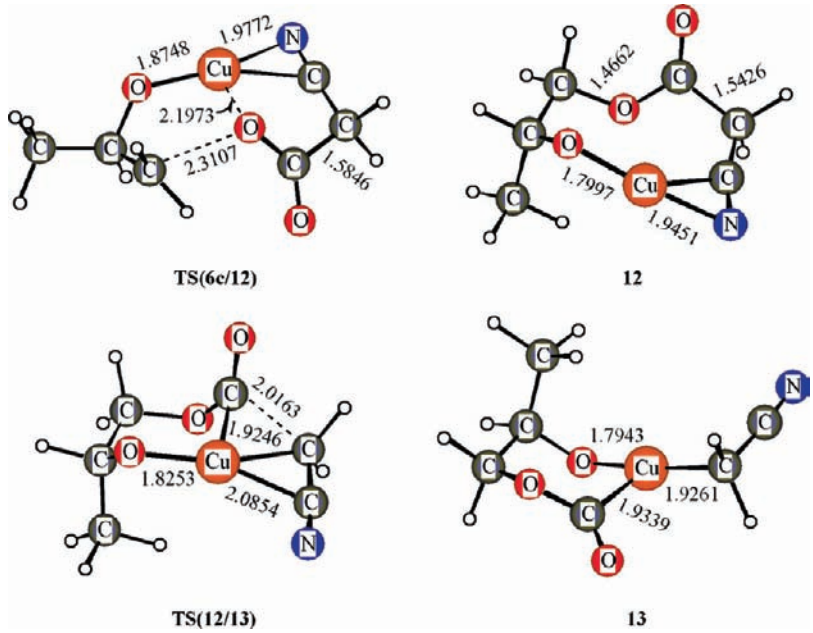

Figure 6. The optimized geometries of the species involved in path 1-B. The bond lengths are in angstroms.

Finally, the electrophilic attack of the C_3 atom on the $O_{epoxide}$ atom results in the formation of the cyclic carbonate and regeneration of the catalyst. As illustrated in Figure 5, in this step, we have located one authentic transition state **TS(10/11)**. Its imaginary frequency is 129.01 cm^{-1}. The IRC calculation shows that the transfer of C_3 atom from Cu to O_3 atoms leads to the cleavage of Cu−C_3 and the formation of C_3−O_3 bond; after the transition state, the most stable complex **11** with the cyclic carbonate (the product molecule) coordinated to the copper atom through the oxygen atom is given. The Cu−C and Cu−O distances are 1.9058 and 1.9287 Å in **11**, respectively. In **11**, the Wiberg bond index of Cu−O bond is 0.1338, which indicates that there is a weak interaction between cyclic carbonate and $CuCH_2CN$ fragment. The calculated energy barrier from **10** to **TS(10/11)** is 2.24 kcal/mol, which implies that this transformation can take place very easily. The transition state **TS(10/11)** is related to the dissociation of the product molecule (cyclic carbonate) and regeneration of the catalyst. This step (**10** → **11**) is highly exothermic by 25.11 kcal/mol.

Path 2. Taking the more active carbon dioxide carrier **7** as the starting point, a propylene oxide molecule can also coordinate to the electrophilic copper atom through the $O_{epoxide}$ atom to afford precursor complexes (**7a**, **7b**, **7c**, and **7d**). These complexes are divided into two type enantiomers (type (i), **7a** and **7b**; type (ii), **7c** and **7d**) in the same rule of path 1. The corresponding structures and selected parameters are given in Figure 7. As shown in Figure 7, structures **7c** and **7d** are more stable than **7a** and **7b** by 1.35 kcal/mol, and the former is obviously the favored coordinating mode. However, in **7a** (or **7b**), the $O_{epoxide}$−C_4 bond is more activated than that in **7c** (or **7d**), indicated by the longer C_4−O_3 bond length (1.4620 vs 1.4614 Å) with respect to that of 1.4326 Å in the free propylene oxide. This suggests that **7a** (or **7b**) favors the following reaction of ring-opening of epoxide. The transformations of these isomers

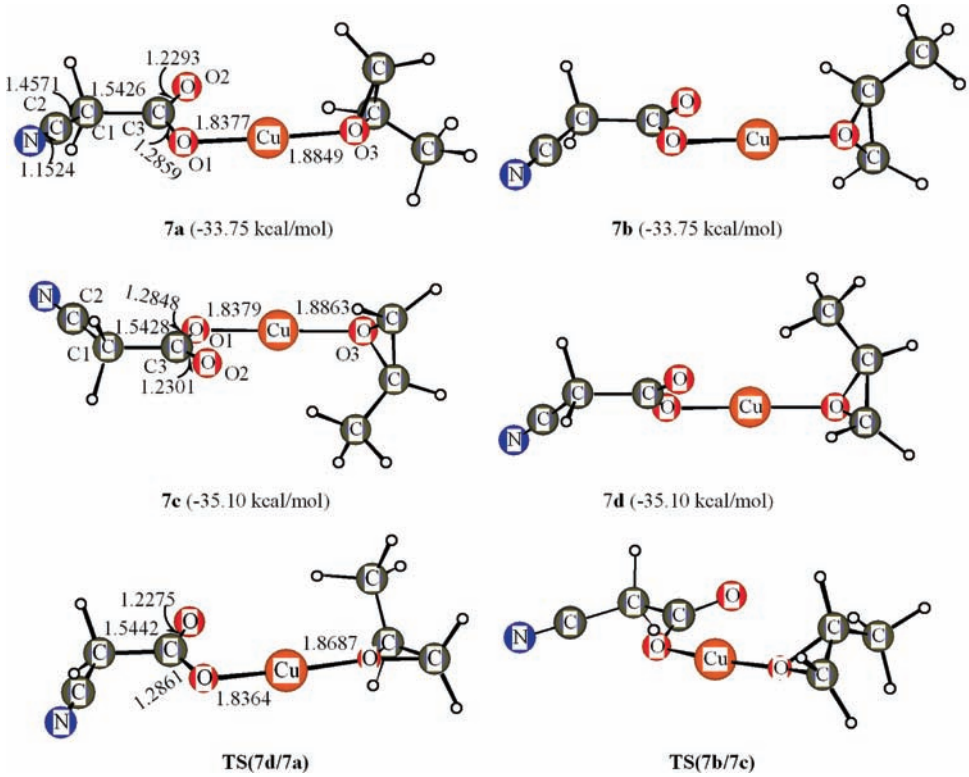

Figure 7. Optimized geometries of epoxide coordination complexes via oxygen atom interacting with carrier **7** and selected parameters. The bond lengths are given in angstroms.

were also investigated via the rotation of propylene oxide. As anticipated, two transition states **TS(7b/7c)** and **TS(7d/7a)** were located, and the corresponding energy barriers are 4.84 and 5.26 kcal/mol. It is worth pointing out that only structures **7a** and **7c** are appropriate to the following ring-opening of the epoxide, which will be testified in the subsequent process. Hence, structures **7b** and **7d** were isomerized to structures **7a** and **7c**, respectively. The net result is that only two isomers (**7a** and **7c**) exist in the reaction system (**7** + epoxide). To examine the reactivity of **7a** and **7c**, we have comprehensively studied two sub-branched pathways, that is, path 2-A and path 2-B. The optimized structures and selected parameters are presented in Figures 8 and 9.

The ring-opening of the epoxide in complex **7a** (or **7c**) to afford **14** (or **20**) can take place via the transition state **TS(7a/14)** (or **TS(7c/20)**). In this step, the carbon atom of CH_2 moiety attacks the adjacent copper atom to bring a four-membered ring intermediate. IRC calculations confirm that **TS(7a/14)** connects **7a** and **14**, while **TS(7c/20)** connects **7c** and **20**. The activation energy barrier from **7a** to **TS(7a/14)** is 11.40 kcal/mol, which is lower by 0.51 kcal/mol than that from **7c** to **TS(7c/20)**. The intermediate **14** is slightly more stable than the intermediate **20** by 0.13 kcal/mol. The next step corresponds to the cycloreversion of the intermediate **14** (or **20**) to yield another ring intermediate **15** (or **21**) via the transition state **TS(14/15)** (or **TS(20/21)**). During the course of **14** to **15**, the torsion of the CH_2 group of epoxide to the oxygen atom of carbon dioxide occurs with the cleavage of $Cu-C_4$. This step is endothermic by 13.49 (**14** → **15**) or 13.36 (**20** → **21**) kcal/mol, with the activation energy of 29.27 or 28.21 kcal/mol, respectively. Although intermediate **15** is slightly less stable than intermediate **21** by 0.21 kcal/mol, the former obviously facilitates the subsequent tautomerization reaction because of the smaller steric hindrance. It is necessary to point out that intermediate **21** did not proceed to the subsequent reaction. Thus, we come to the conclusion that type (ii) complexes are unreactive in the whole reaction process 2 for all three pathways.

As depicted in Figure 8, intermediates **15** and **16** are rotational isomers, which were connected by the transition state **TS(15/16)**. This step is slightly endergonic by 1.83 kcal/mol, while endothermic by 1.95 kcal/mol. The free energy profile in Figure 12 shows that the rotation barrier from **15** to **TS(15/16)** is rather small, which implies this transformation easily takes place. From the intermediate **16**, we suppose that Cu atom may interact with the close-by cyanomethyl C atom. To verify this supposition, we have located the transition state **TS(16/17)**. The imaginary frequency is 135.80i cm^{-1}. IRC calculation indicates that the migration of Cu atom to C_2 is accompanied by a simultaneous cleavage of $Cu-C_3$ and $Cu-O_3$ bonds. The energy barrier from **16** to **TS(16/17)** is only 3.76 kcal/mol. After the reaction overcame **TS(16/17)**, the eight-membered ring intermediate **17** is formed. This step is exergonic by 21.91 kcal/mol (**16** → **17**), while exothermic by 23.71 kcal/mol. Note that intermediates **17** and **9** are a pair of isoenergetic enantiomers.

The following step shows the isomerization of **17** proceeds by the cyanomethyl group remotion from the copper atom, as is similar to the third step in path 1. The transition state **TS(17/18)** was located. IRC results indicate that the migration of Cu atom to C_3 is accompanied by a simultaneous cleavage of C_3-C_1. After the reaction overcame **TS(17/18)**, the six-membered ring intermediate **18** is formed. This step is endothermic by 20.96 (**17** → **18**) kcal/mol, with the activation energy of 36.16 kcal/mol. It is worth noting that the ring-closure in **17** occurs due to the main interaction between the lobe of the p orbital in C_3 of HOMO and the d orbital in copper atom of LUMO. The last step involves electrophilic attack of the C_3 atom on the $O_{epoxide}$ atom, which is similar to that in path 1. One authentic transition state **TS(18/19)** was located, and its imaginary frequency is 127.08 cm^{-1}. The IRC calculation indicates that the motion of C_3 atom from Cu to O_3 atoms leads

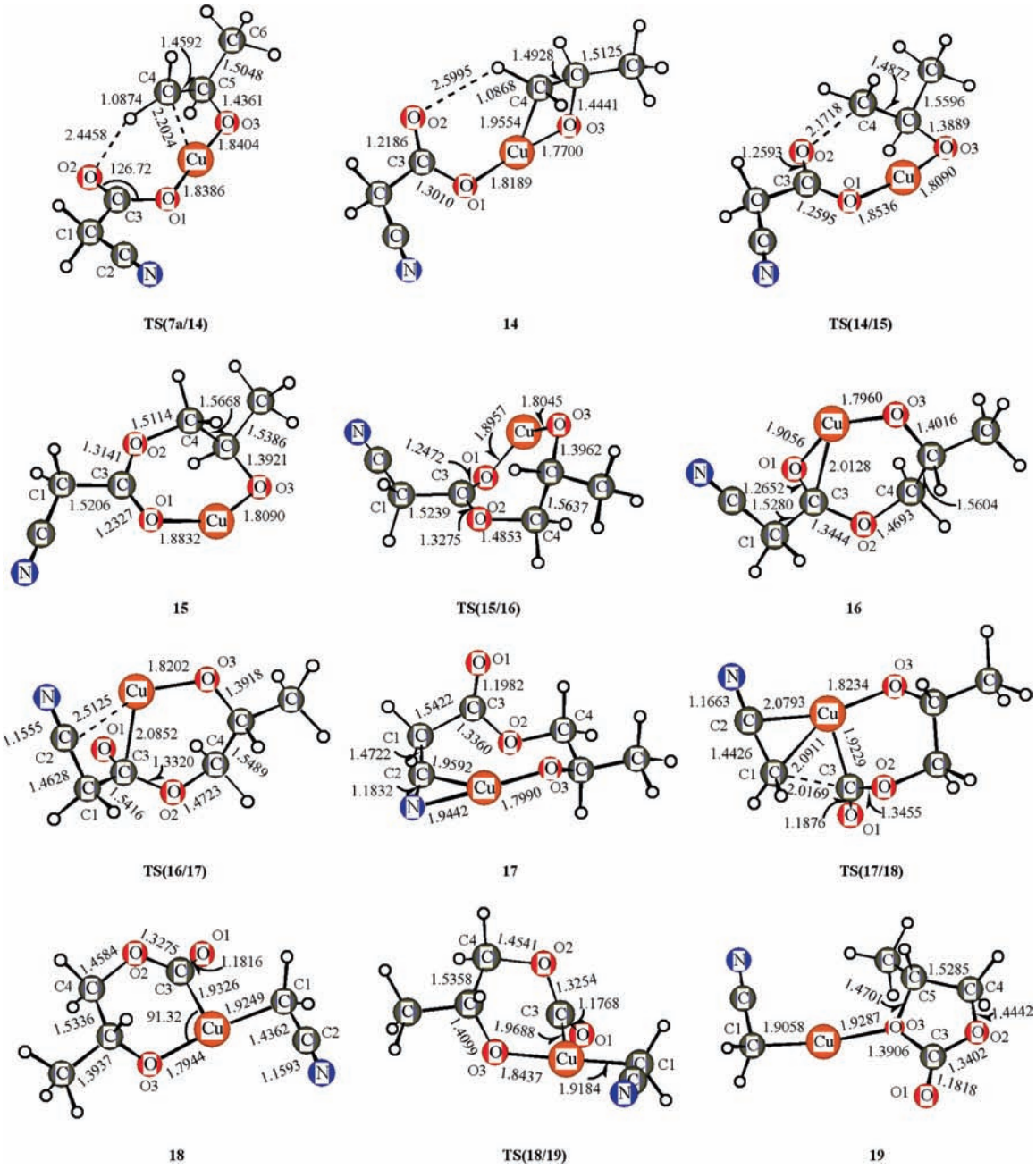

Figure 8. Key structures involved in the mechanism of the reaction of propylene oxide with carbon dioxide carrier **7** in the gas phase and selected parameters. The bond lengths are given in angstroms.

to the cleavage of Cu−C_3 and the formation of C_3−O_3 bond; after the transition state **TS(18/19)**, the cyclic carbonate coordinated to the copper atom through the oxygen atom is produced while the catalyst is regenerated. As compared to complex **7a**, product complex **19** is lower in free energy by 4.44 kcal/mol. The calculated energy barrier from intermediate **18** to the transition state **TS(18/19)** is 2.17 kcal/mol, which is slightly lower by 0.07 kcal/mol than that from **10** to **TS(10/11)** in path 1. It is indicated that the production of cyclic carbonate from **18** to **19** can proceed very facilely than from **10** to **11**.

Path 3. For the third pathway, a propylene oxide molecule coordinates to the electrophilic copper atom of the most active carbon dioxide carrier **8** through the $O_{epoxide}$ atom, where two types of enantiomers (type (i), **8a** and **8b**; type (ii), **8c** and **8d**) are also produced. The corresponding structures and selected parameters are given in Figure 10.

Similarly, complexes **8c** and **8d** are more stable than **8a** and **8b** by 1.29 kcal/mol, and the former is obviously the favored coordinating mode. However, in **8a** (or **8b**), the $O_{epoxide}$−C_4 bond is more activated than that in **8c** (or **8d**), indicated by the longer C_4−O_3 bond length (1.4636 vs 1.4624 Å) with respect to that of 1.4326 Å in the free propylene oxide. This implies that **8a** and **8b** favor the subsequent reaction of ring-opening of epoxide. As discussed in path 2, we can draw a conclusion that type (ii) complexes are not reactive in the process for the production of propylene carbonate. Hereby, there is no need to investigate the subsequent development of complexes **8c** and **8d**. Also, in the following reaction process, it is proved that **8b** is not appropriate to proceed, so the effective precursor complex is **8a**. It is worthy of note that **8a** is more stable by 0.31 kcal/mol than **7a**. Is conformation **8a** preferred in the whole catalytic cycle?

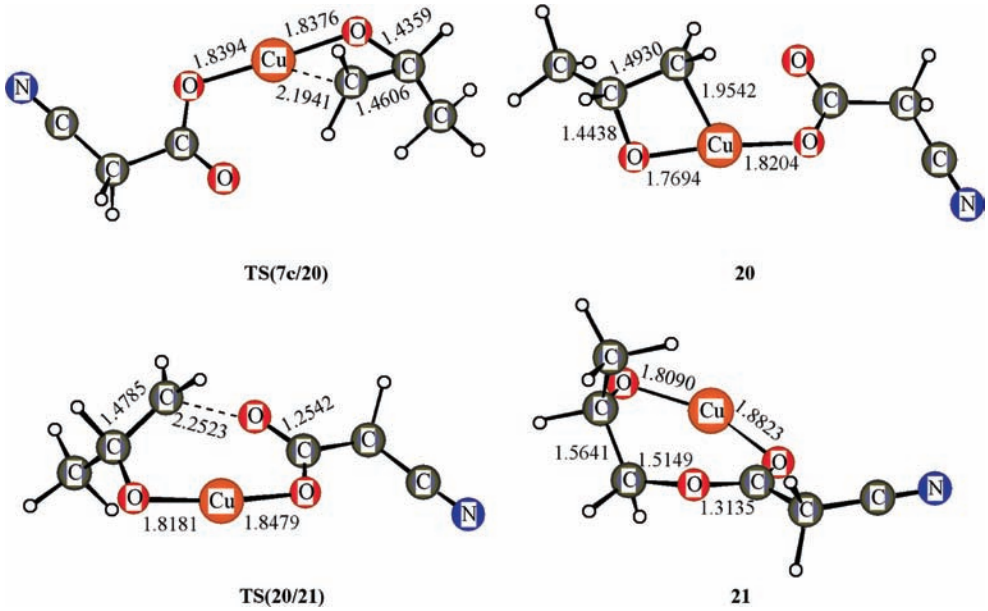

Figure 9. The optimized geometries of the species involved in path 2-B. The bond lengths are in angstroms.

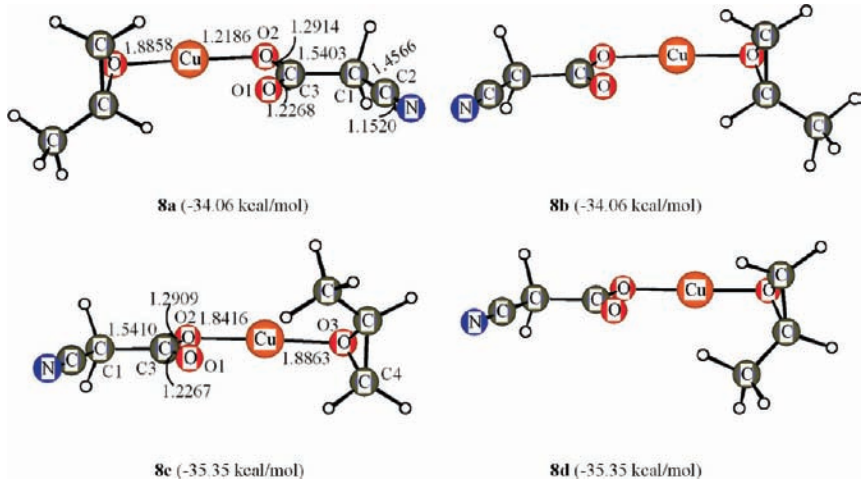

Figure 10. Optimized geometries of epoxide coordination complexes via oxygen atom interacting with carrier **8** and selected parameters. The bond lengths are given in angstroms.

As illustrated in Figure 11, the ring-opening of the epoxide in complex **8a** proceeds by CH_2 moiety migrating and attacking on the adjacent copper atom. The calculations show that this process goes ahead via the transition state **TS(8a/22)**. The activation energy barrier from **8a** to **TS(8a/22)** is 11.51 kcal/mol, which is slightly higher by 0.11 kcal/mol than that from **7a** to **TS(7a/14)**. The intermediate **22** is slightly less stable by 0.11 kcal/mol than the intermediate **14**. The next step corresponds to the further cycloreversion of the four-membered ring intermediate **22** to yield a seven-numbered ring intermediate **23** via the transition state **TS(22/23)**. The activation energy barrier from **22** to **TS(22/23)** is 28.37 kcal/mol, which is lower by 0.90 kcal/mol than that from **14** to **TS(14/15)**. Obviously, the whole ring-opening of the epoxide in **8a** is easier than that of **7a**, due to a lower free energy barrier. This step is endergonic by 16.60 kcal/mol, while endothermic by 13.65 kcal/mol.

The subsequent step is the geometry shrinking process from intermediate **23** to **24**. The transition state **TS(23/24)** was located. Its imaginary frequency is 58.71 cm^{-1}; the corresponding vibrational mode indicates the copper atom does not vibrate, but the rest vibrates. The calculated energy barrier from **23** to **TS(23/24)** is 4.47 kcal/mol. This step is also endergonic by 3.34 kcal/mol. It is noted that the intermediate **24** is slightly less stable than intermediate **16**, while it would facilitate matters if the former transformed the latter. In this step, we have located the transition state **TS(24/16)**, which connects **24** and **16**. The imaginary frequency is 38.78i cm^{-1}, associated with the rotation of cyanomethyl group around the C_1-C_3 bond. The energy barrier from **24** to **TS(24/16)** is 2.30 kcal/mol, which implies that this step proceeds very easily. After the reaction overcame **TS(24/16)**, the following steps are just the same with the latter steps starting from intermediate **16** in path 2.

To gain a complete understanding of the mechanistic pathways, the free energy profiles obtained with the three mechanisms, shown in Figure 12, must be compared. By comparing the energetics of paths 1, 2, and 3 described above, one can find that path 3 is preferred, because the activation energy barrier of the ring-opening of the epoxide is the lowest among three paths. Also, the energies of **6a**, **7a**, and **8a** are below those of the reactants (**1** + CO_2 + epoxide) by 29.59, 33.75, and 34.06 kcal/mol, respectively. Here, it is worth mentioning that more reliable single-point energy calculations were performed on the species involved in paths 2 and 3 by the MP2/6-311+G** method. The general trend of the MP2 Gibbs free energy profiles

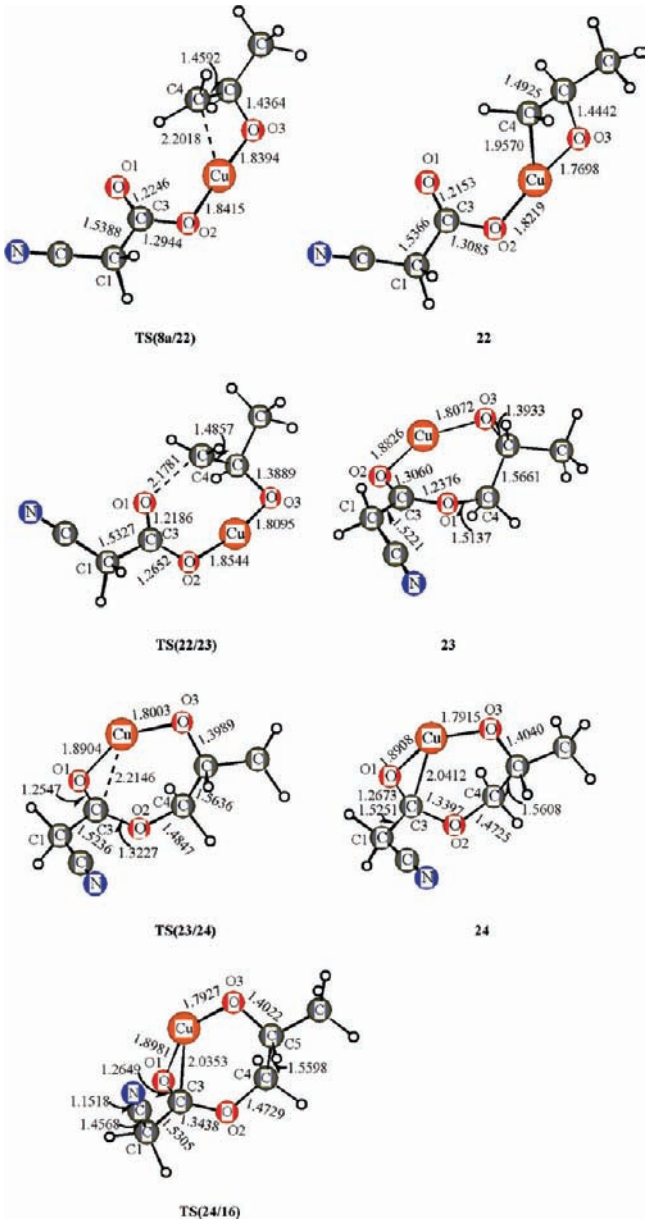

Figure 11. Key structures involved in the mechanism of the reaction of propylene oxide with carbon dioxide carrier **8** in the gas phase and selected parameters. The bond lengths are given in angstroms.

for paths 2 and 3 (see Figure S2) is very similar to that of the B3LYP energy profiles in the bottom of Figure 12. Therefore, the computation method (B3LYP/6-311G**) used in this study is more reliable in studying trends than providing absolute numbers for the reactions. Our results clearly indicate that the epoxide coordinating to **8** is essentially more favorable than to **6** and **7**. On the basis of the energetic profiles (see Figures 3 and 12), the overall reaction is exothermic, and the rate-determining step is the eight-membered ring intermediate **17** oxidation transformation. The experiments performed by Saegusa et al.[15] show that the presence of the electron-withdrawing group ligand on copper leads to higher yield. It is expected that the electron-withdrawing group, which shifts electron density from copper atom toward the CN moiety so that increases the electrophilicity of the copper of reactant, should reduce the barrier to the formation of the activated carbon dioxide carrier in process 1. The electron-withdrawing group should also facilitate the ring-opening in **16** because this step is related to the interaction between copper and cyanomethyl C_2 atom.

As can be seen from Figure 12, the reaction pathway involves $O_{epoxide}-C$ and $C_{carbondioxide}-C_{cyanomethyl}$ bonds cleavage, which cause larger charge separation and partly result in the high reaction barriers. It is well recognized that gas-phase calculations, which are now commonly carried out in computational chemistry, for such charge separation processes always produce very high reaction barriers.[29] Very interestingly, intermediate **17** was predicted by the calculations to be stable but not observed experimentally. We suspect that the calculations might have overestimated the electrostatic interactions between the copper and cyano group.

In addition, the frontier molecular orbital (FMO) analysis has been successful in accounting for a range of addition reactions. According to the FMO theory,[30] the reaction should be governed by the energy difference between the HOMO of one reactant and the LUMO of the other. Herein, we examined the FMO energy difference between reactants at the B3LYP/6-311G** level. As shown in Table 1, the energy difference (ΔF MO_A) between LUMO of **6** (**7** or **8**) and HOMO of epoxide is smaller than the corresponding energy difference (ΔF MO_B) between LUMO of epoxide and HOMO of **6** (**7** or **8**). Thus, the addition reaction for **6** (**7** or **8**) and epoxide systems is dominated by a relatively small energy gap between LUMO of **6** (**7** or **8**) and HOMO of epoxide. The frontier orbitals of **6**, **7**, **8**, and epoxide are illustrated in Figure 13. The greater orbital percentage contribution of copper in the LUMO of carbon dioxide carrier explains the preference for epoxide coordinating to **8** over **6** and **7**, which is demonstrated by the lowest ΔF MO_A energy gap (0.16407 au) between LUMO of **8** and HOMO of epoxide. Here, we should mention that the strong electrostatic interaction between the positively charged Cu atom in **6** (**7** or **8**) and the negatively charged O atom in epoxide accelarates the epoxide−**6** (**7** or **8**) bonding, but it is not dominating factor. Actually, the HOMO of epoxide and the LUMO of **6**, **7**, and **8** mainly constitute epoxide−**6** (**7** or **8**) bonding. On the basis of the above analysis, it is concluded that species **8** is the best carbon dioxide carrier. The orbital symmetry also explains that the O−C−C plane of epoxide cannot approach parallel to the Cu−O bond, and thus the perpendicular precursor complexes are obtained.

An examination of the natural populations reveals an interesting change for the Cu atoms. The charges of Cu along with the preferred pathway are depicted in Figure 14. As all of the catalytic events occur on the Cu atom, the charge on the Cu atom increases in the ring-opening of epoxide step, and then decreases in the methylene oxidative addition step (**22** → **23**). The variations of the charges on Cu atom directly affect the Cu coordination geometry. For example, the center ion coppers of intermediates **22**, **24**, **16**, and **18** are capable of attaining 3-fold coordination with triangular planar or pyramidal geometries. However, the Cu atoms in intermediates **8a**, **23**, and **17** display 2-fold coordination with linear or angle geometries. As shown in Figure 14, the variations of the charges clearly imply that the copper atom serves as an orbital or charge reservoir.

Conclusion

The complete catalytic cycle of the coupling reaction of propylene oxide with carbon dioxide employing $NCCH_2Cu$ as an active catalyst has been investigated at the B3LYP level of theory. All species involved in the catalytic cycle have been fully characterized to be energy minimum structures for the intermediates or saddle point structures for the transition states. Our results reveal that the overall reaction is stepwise and considered to include two processes. In process 1, CO_2 insertion

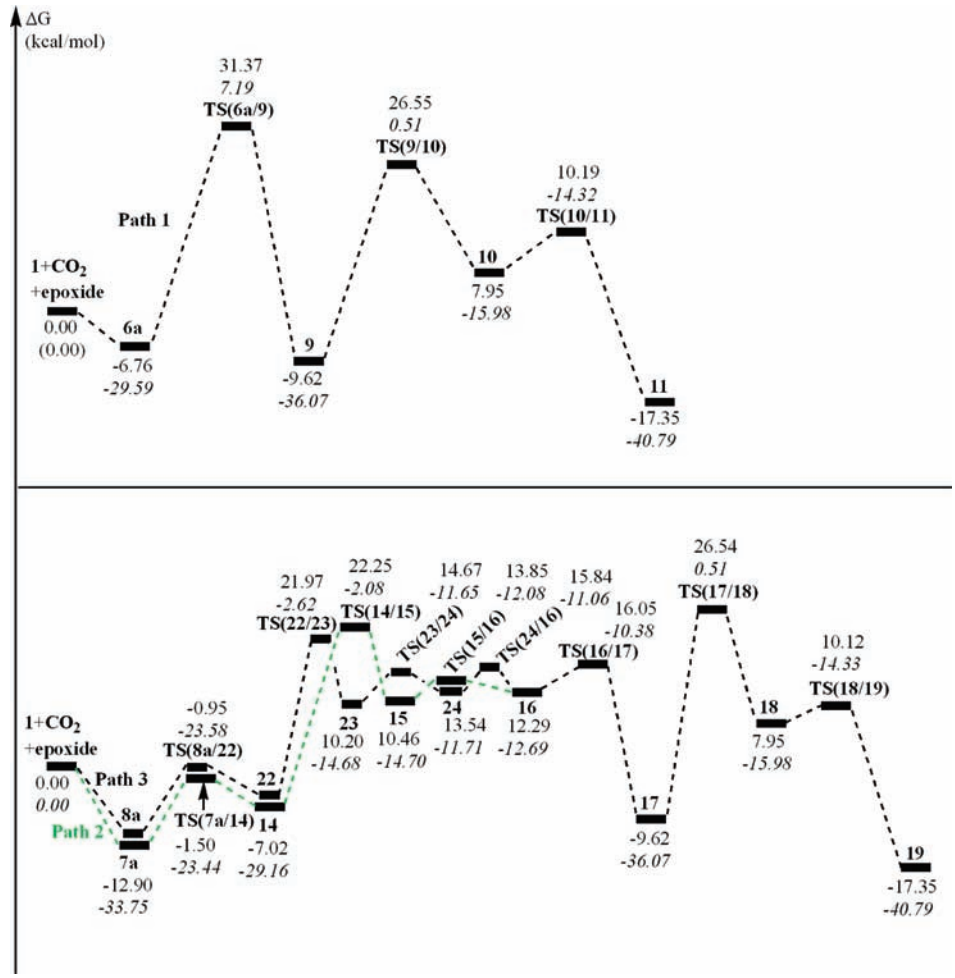

Figure 12. Schematic free energy profiles (in kcal/mol) for the reaction of propylene oxide with carbon dioxide carriers **6** (top line, path 1), **7** (dashed green line, path 2), and **8** (dashed black line, path 3) in process 2 in the gas phase. The calculated relative electronic energies (values in italic) are also given.

TABLE 1: Frontier Molecular Energies (au) for the Reactants and Their Differences between the Reactants Computed by the B3LYP/6-311G Method**[a]

reactants	$HOMO_I$	$LUMO_I$	$HOMO_{II}$	$LUMO_{II}$	ΔF MO_A	ΔF MO_B
6 + epoxide	−0.24291	−0.07935	−0.26965	0.04925	0.1903	0.29216
7 + epoxide	−0.24015	−0.10447	−0.26965	0.04925	0.16518	0.2894
8 + epoxide	−0.24074	−0.10558	−0.26965	0.04925	0.16407	0.28999

[a] ΔF MO_A = energy difference between $LUMO_I$ of the corresponding isomer (**6**, **7**, or **8**) and $HOMO_{II}$ of epoxide. ΔF MO_B = energy difference between $LUMO_{II}$ of epoxide and $HOMO_I$ of the corresponding isomer (**6**, **7**, or **8**).

into the Cu(I)−C bond of copper(I) cyanomethyl affords activated carbon dioxide carriers. The first step, that is, carbon dioxide reacts with species **1** to produce the complex **5** via directly side-on attack, determines the rate in process 1. In process 2, the epoxide coordination to carriers of activated CO_2 can take place via three possible reaction pathways. In the first case (path 1), the most stable activated carbon dioxide carrier **6** was reacted to one propylene oxide molecule. The second path (path 2) is about the reaction between the more active carbon dioxide carrier **7** and propylene oxide. For the third path (path 3), the most active carbon dioxide carrier **8** interacted with one propylene oxide molecule. From the calculated barrier heights and reaction energies, one can note path 3 is more favored. Kinetically, the ring-opening of epoxide to copper atom forming the four-membered ring intermediates **14** (path 2) and **22** (path 3) is more favored than that to the $O_{carbondioxide}$ atom to form the eight-membered ring intermediate **9** (path 1), as indicated by the free energy barriers of 11.40, 11.51, and 38.13 kcal/mol, respectively. Thermodynamically, the electronic energy of **8a** is slightly lower by 0.31 kcal/mol than that of **7a**. Therefore, the best activated carbon dioxide carrier is species **8**. The overall reaction is exothermic.

Also, some other new points have been clarified. (1) The CO_2 concentration or partial pressure is helpful for the transformation of carbon dioxide carrier species to the product cyclic carbonate. (2) Natural bond orbital (NBO) analysis results show that the copper atom serves as an orbital or charge reservoir in the overall reaction. (3) The calculated free energy barriers imply that the catalytic activity of $NCCH_2Cu$ is preferable. (4) The eight-membered ring intermediate oxidation transformation in process 2 effectively demonstrates the cooperativity of CH_2CN moiety with the catalytic center copper. These results could explain satisfactorily the reported experimental observations of why

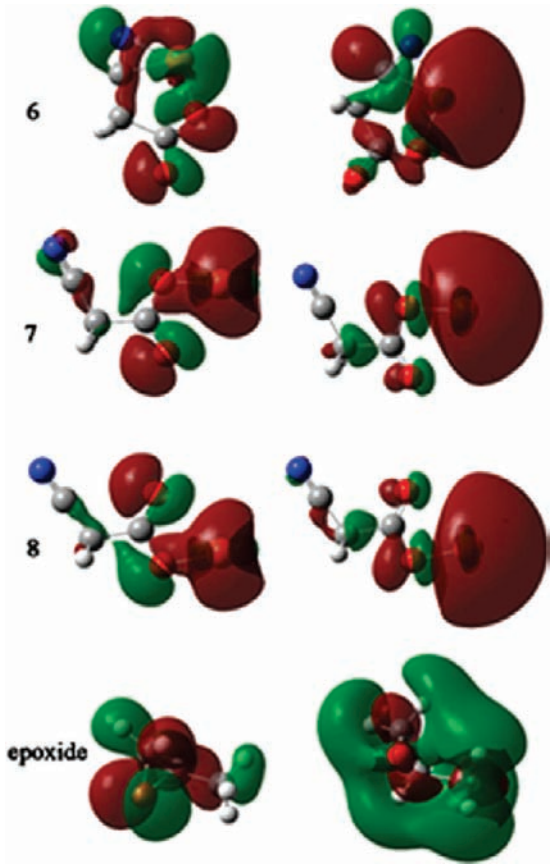

Figure 13. Front orbitals of **6**, **7**, **8**, and epoxide (left, HOMO; right, LUMO).

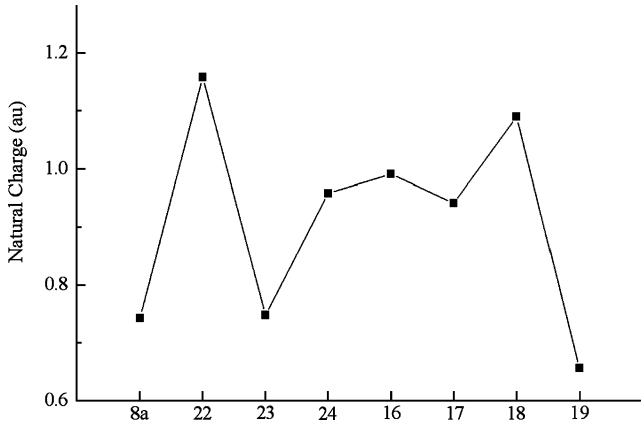

Figure 14. Natural charges of Cu atom for the preferred pathway (path 3) in process 2.

$NCCH_2Cu$ plays an important role in the formation of propylene carbonate at high temperature.

Acknowledgment. This work was supported by the Natural Science Foundation of China (20673070).

Supporting Information Available: Figures S1 and S2, Schemes S1−3, complete ref 25, Tables S1−4 with total electronic energies and zero-point energies (ZPE) as well as thermal corrections to enthalpies and Gibbs free energies (403.15 K, 40 atm), and the optimized Cartesian coordinates. This material is available free of charge via the Internet at http://pubs.acs.org.

References and Notes

(1) Leitner, W. *Coord. Chem. Rev.* **1996**, *155*, 257.
(2) Marks, T. J.; et al. *Chem. Rev.* **2001**, *101*, 953.
(3) Shaikh, A. A. G.; Sivaram, S. *Chem. Rev.* **1996**, *96*, 951.
(4) See, for example: (a) Paddock, R. L.; Ngugen, S. T. *J. Am. Chem. Soc.* **2001**, *123*, 11498. (b) Yamaguchi, K.; Ebitani, K.; Yoshida, T.; Yoshida, H.; Kaneda, K. *J. Am. Chem. Soc.* **1999**, *121*, 4526. (c) Yano, T.; Matsui, H.; Koiki, T.; Ishiguro, H.; Fujihara, H.; Yoshihara, M.; Maeshima, T. *Chem. Commun.* **1997**, 1129. (d) Darensbourg, D. J.; Holtcamp, M. W. *Coord. Chem. Rev.* **1996**, *153*, 155. (e) Fujinami, T.; Suzuki, T.; Kamiya, M.; Fukuzawa, S.; Sakai, S. *Chem. Lett.* **1985**, *14*, 199. (f) Kim, H. S.; Kim, J. J.; Lee, B. G.; Jung, O. S.; Jang, H. G.; Kang, S. O. *Angew. Chem., Int. Ed.* **2000**, *39*, 4096. (g) Kruper, W. J.; Deller, D. V. *J. Org. Chem.* **1995**, *60*, 725. (h) Kawanami, H.; Ikushima, Y. *Chem. Commun.* **2000**, 2089. (i) Caló, V.; Nacci, A.; Monopoli, A.; Fanizzi, A. *Org. Lett.* **2002**, *4*, 2561. (j) Kihara, N.; Hara, N.; Endo, T. *J. Org. Chem.* **1993**, *58*, 6198. (k) Li, F.; Xia, C.; Xu, L.; Sun, W.; Chen, G. *Chem. Commun.* **2003**, 2042. (l) Lu, X.-B.; Liang, B.; Zhang, Y.-J.; Tian, Y.-Z.; Wang, Y.-M.; Bai, C.-X.; Wang, H.; Zhang, R. *J. Am. Chem. Soc.* **2004**, *126*, 3732. (m) Shen, Y.-M.; Duan, W.-L.; Shi, M. *J. Org. Chem.* **2003**, *68*, 1559. (n) Li, F.; Xiao, L.; Xia, C.; Hu, B. *Tetrahedron Lett.* **2004**, 8307. (o) Jiang, J.-L.; Gao, F.; Hua, R.; Qiu, X. *J. Org. Chem.* **2005**, *70*, 381. (p) Shen, Y.-M.; Duan, W.-L.; Shi, M. *Eur. J. Org. Chem.* **2004**, 3080. (q) Huang, J.-W.; Shi, M. *J. Org. Chem.* **2003**, *68*, 6705. (r) Jing, H.; Edulji, S. K.; Gibbs, J. M.; Stern, C. L.; Zhou, H.; Nguyen, S. T. *Inorg. Chem.* **2004**, *43*, 4315. (s) Sit, W. N.; Ng, S. M.; Kwong, K. Y.; Lau, C. P. *J. Org. Chem.* **2005**, *70*, 8583. (t) Man, M. L.; Lam, K. C.; Sit, W. N.; Ng, S. M.; Zhou, Z.; Lin, Z.; Lau, C. P. *Chem.-Eur. J.* **2006**, *12*, 1004.
(5) (a) Aida, T.; Inoue, S. *J. Am. Chem. Soc.* **1983**, *105*, 1304. (b) Kojima, F.; Aida, T.; Inoue, S. *J. Am. Chem. Soc.* **1986**, *108*, 391. (c) Hirai, Y.; Aida, T.; Inoue, S. *J. Am. Chem. Soc.* **1989**, *111*, 3062. (d) Komatsu, M.; Aida, T.; Inoue, S. *J. Am. Chem. Soc.* **1991**, *113*, 8492.
(6) (a) Carmona, E.; Palma, P.; Paneque, M.; Poveta, M. L. *J. Am. Chem. Soc.* **1986**, *108*, 6424. (b) Carmona, E.; Gutihez-Puebla, E.; Marin, J. M.; Monge, A.; Paneque, M.; Poveta, M. L.; Ruiz, C. *J. Am. Chem. Soc.* **1989**, *111*, 2883.
(7) Braunstein, P.; Matt, D.; Nobel, D. *J. Am. Chem. Soc.* **1988**, *110*, 3207.
(8) (a) Darensbourg, D. J.; Grotsch, G. *J. Am. Chem. Soc.* **1985**, *107*, 7473. (b) Darensbourg, D. J.; Ovalles, C. *J. Am. Chem. Soc.* **1987**, *109*, 3330.
(9) Aye, K. T.; Gelmini, L.; Payne, N. C.; Vittal, J. J.; Puddephatt, R. J. *J. Am. Chem. Soc.* **1990**, *112*, 2464.
(10) (a) Amatore, C.; Jutand, A. *J. Am. Chem. Soc.* **1991**, *113*, 2819. (b) Amatore, C.; Jutand, A. *J. Electroanal. Chem.* **1991**, *306*, 141.
(11) Tsai, J. C.; Nicholas, K. M. *J. Am. Chem. Soc.* **1992**, *114*, 5117.
(12) (a) Sakaki, S.; Ohkubo, K. *Inorg. Chem.* **1988**, *27*, 2020. (b) Sakaki, S.; Ohkubo, K. *Inorg. Chem.* **1989**, *28*, 2583. (c) Sakaki, S.; Ohkubo, K. *Organometallics* **1989**, *8*, 2970.
(13) Sakaki, S.; Musashi, Y. *Inorg. Chem.* **1995**, *34*, 1914.
(14) Braustein, P.; Matt, D.; Nobel, D. *Chem. Rev.* **1988**, *88*, 747.
(15) Tsuda, T.; Chujo, Y.; Saegusa, T. *J. Chem. Soc., Chem. Commun.* **1976**, 415.
(16) Chisholm, M. H.; Cotton, F. A.; Extine, M. W.; Reichert, W. W. *J. Am. Chem. Soc.* **1978**, *100*, 1727.
(17) Tsuda, T.; Chujo, Y.; Saegusa, T. *J. Am. Chem. Soc.* **1978**, *100*, 630.
(18) Gambarotta, S.; Floriani, C.; Chiesi-Villa, A.; Guastini, C. *J. Am. Chem. Soc.* **1985**, *107*, 2985.
(19) Aye, K.-T.; Ferguson, G.; Lough, A. J.; Puddephatt, R. J. *Angew. Chem., Int. Ed.* **1989**, *28*, 767.
(20) (a) Becke, A. D. *J. Chem. Phys.* **1993**, *98*, 5648. (b) Miehlich, B.; Savin, A.; Stoll, H.; Preuss, H. *Chem. Phys. Lett.* **1989**, *157*, 200. (c) Lee, C.; Yang, W.; Parr, G. *Phys. Rev. B* **1988**, *37*, 785. (d) Stephens, P. J.; Devlin, F. J.; Chabalowski, C. F. *J. Phys. Chem.* **1994**, *98*, 11623.
(21) (a) Gonzalez, C.; Schlegel, H. B. *J. Chem. Phys.* **1989**, *90*, 2154. (b) Gonzalez, C.; Schlegel, H. B. *J. Phys. Chem.* **1990**, *94*, 5523.
(22) Hay, P. J.; Wadt, W. R. *J. Chem. Phys.* **1985**, *82*, 299.
(23) Krishnan, R.; Binkley, J. S.; Seeger, R.; Pople, J. A. *J. Chem. Phys.* **1980**, *72*, 650.
(24) Reed, E.; Curtiss, L. A.; Weinhold, F. *Chem. Rev.* **1988**, *88*, 899.
(25) Frisch, M. J.; Trucks, G. W.; Schlegel, H. B.; Scuseria, G. E.; Robb, M. A.; Cheeseman, J. R.; *Gaussian 03*, revision C.01; Gaussian, Inc.: Wallingford, CT, 2004.
(26) Himo, F.; Lovell, T.; Hilgraf, R.; Rostovtsev, V. V.; Noodleman, L.; Sharpless, K. B.; Fokin, V. V. *J. Am. Chem. Soc.* **2005**, *127*, 210.
(27) (a) Zhao, H.; Lin, Z.; Marder, T. B. *J. Am. Chem. Soc.* **2006**, *128*, 15637. (b) Dang, L.; Zhao, H.; Lin, Z.; Marder, T. B. *Organometallics* **2007**, *26*, 2824.
(28) Versluis, L.; Ziegler, T.; Fan, L. *Inorg. Chem.* **1990**, *29*, 4530.
(29) Cordaro, J. G.; Bergman, R. G. *J. Am. Chem. Soc.* **2004**, *126*, 16912.

(30) (a) Fukui, K.; Fujimoto, H. In *Mechanisms of Molecular Migrations*; Thyagarajan, B. S., Ed.; Interscience: New York, 1968; Vol. 2. (b) Fukui, K. *Acc. Chem. Res.* **1971**, *4*, 57. (c) Fukui, K. *Angew. Chem., Int. Ed. Engl.* **1982**, *21*, 801.

(31) Liu, Z.; Torrent, M.; Morokuma, K. *Organometallics* **2002**, *21*, 1056–1071.

(32) Sun, H.; Zhang, D. *J. Phys. Chem. A* **2007**, *111*, 8036.

(33) Fraile, J. M.; García, J. I.; Martínez-Merino, V.; Mayoral, J. A.; Salvatella, L. *J. Am. Chem. Soc.* **2001**, *123*, 7616.

(34) Zhou, M.; Zhang, L.; Chen, M.; Zheng, Q.; Qin, Q. *J. Phys. Chem. A* **2000**, *104*, 10159.

(35) Rauhut, G.; Pulay, P. *J. Phys. Chem.* **1995**, *99*, 3093.

JP809471S